RSC Advances

PAPER

View Article Online
View Journal | View Issue

Cite this: *RSC Adv.*, 2025, **15**, 37518

Breaking the p-type doping barrier in β-Ga_2O_3: a GaN-based heterojunction bipolar transistor with high gain, high breakdown, and RF capability

Phuc Hong Than, *[a] Tho Quang Than[b] and Yasushi Takaki[c]

Despite extensive research on unipolar β-Ga_2O_3 semiconductor devices, the advancement of bipolar devices, particularly heterojunction bipolar transistors (HBTs), has been significantly hindered by the lack of reliable p-type doping in β-Ga_2O_3. In this paper, we present the first comprehensive simulation study of a functional HBT based on an n-type β-Ga_2O_3 emitter, a p-type GaN base, and an n-type GaN collector, aiming to address the critical challenge of p-type doping in β-Ga_2O_3 for bipolar devices. The proposed Ga_2O_3/GaN HBT, simulated with full consideration of traps, exhibits a maximum DC current gain (β_{DC}) of 18.3, a high collector current density (J_C) of 14.3 kA cm^{-2}, a collector–base breakdown voltage (BV_{CBO}) of 120 V, a power figure of merit (PFOM) of 41.3 MW cm^{-2}, and a low specific on-resistance ($R_{on,sp}$) of 0.35 mΩ cm^2. The temperature-dependent current–voltage (I–V) characteristics from 300 K to 460 K reveal stable operation up to 460 K, albeit with a 31.1% reduction in β_{DC} and a 30.0% decline in PFOM due to carrier mobility degradation and enhanced recombination. Furthermore, device performance was optimized by engineering the base and collector thicknesses. The results indicate that a thin base (0.05 μm) maximizes β_{DC}, while a thick collector (2.0 μm) boosts PFOM to 138 MW cm^{-2} without compromising gain. In addition, high-frequency simulations show a cutoff frequency (f_T) of 30 GHz at 300 K, confirming the device's suitability for RF and power-switching applications. These results indicate that the Ga_2O_3/GaN HBT is a promising candidate for next-generation power electronics, owing to its unique combination of high breakdown voltage and excellent frequency performance.

Received 23rd September 2025
Accepted 30th September 2025

DOI: 10.1039/d5ra07197f

rsc.li/rsc-advances

1 Introduction

Among wide-bandgap semiconductors such as silicon carbide (SiC), gallium nitride (GaN), and gallium oxide (Ga_2O_3), beta-gallium oxide (β-Ga_2O_3) has garnered significant attention due to its ultra-wide bandgap of ~4.8 eV, high breakdown electric field exceeding 8 MV cm^{-1}, excellent controllability of n-type conductivity through intentional donor doping over a broad carrier concentration range (10^{15}–10^{20} cm^{-3}), and the availability of large-area, low-defect single-crystal substrates grown by melt-based techniques, which are compatible with various epitaxial growth methods.[1–6] Thus, over the past decade, extensive research and development has focused on unipolar devices based on β-Ga_2O_3 for next-generation high-power and high-frequency applications, such as Schottky barrier diodes (SBDs), metal-oxide-semiconductor field-effect transistors (MOSFETs), and high-electron-mobility transistors (HEMTs).[7–20] Prior research at the National Institute of Information and Communications Technology (NICT, Tokyo, Japan), where one of the authors participated, showed that normally-off lateral β-Ga_2O_3 MOSFETs with nitrogen-doped channels were feasible. The use of nitrogen as a deep acceptor for current-blocking layers in β-Ga_2O_3-based power devices was validated by the stable performance of these devices at a threshold voltage of +5 V.[21,22] However, the lack of reliable p-type doping in β-Ga_2O_3 has significantly limited the development and investigation of bipolar devices based on this material. As a key technology in high-speed electronics, heterojunction bipolar transistors (HBTs) offer superior frequency response and power-handling capabilities compared to other bipolar devices, making them essential for next-generation RF and power-switching applications. Recently, M. Mehta *et al.* proposed the use of p-type oxides to realize HBTs based on β-Ga_2O_3.[23] A β-Ga_2O_3 HBT employing a Cu_2O base was simulated to estimate its power figure of merit (PFOM), but its performance was severely constrained by the low bandgap of Cu_2O. To address this issue, the authors suggested using alternative p-type oxides with a bandgap of E_g > 3.4 eV and an electron diffusion length >0.4 μm to achieve PFOM values exceeding those of state-of-the-art β-Ga_2O_3 unipolar transistors.

[a]*Duy Tan University (DTU), 3 Quang Trung, Hai Chau, Danang 550000, Vietnam. E-mail: thanhongphuc@duytan.edu.vn*

[b]*Central Power Corporation (EVNCPC), 78A Duy Tan, Hoa Thuan Dong, Hai Chau, Danang 550000, Vietnam*

[c]*Power Device Works, Mitsubishi Electric Corporation, 997, Miyoshi, Koushi-shi, Kumamoto 861-1197, Japan*

Promising candidates such as NiO and r-GeO_2 were identified for their potential to significantly enhance PFOM.[23] In this study, we propose a HBT structure based on n-type β-Ga_2O_3 and p-type GaN. GaN was chosen as the base material due to its wide bandgap of 3.53 eV, greater than the 3.4 eV threshold suggested by Mehta *et al.*, and its high compatibility with β-Ga_2O_3.[24,25] Although Ga_2O_3/GaN heterostructures for various unipolar and optoelectronic applications have been widely studied and reported, including photodetectors,[26–28] light-emitting diodes (LEDs),[29–31] gate dielectrics or passivation layers in HEMTs/metal-oxide-semiconductor high-electron-mobility transistors (MOSHEMTs),[25,32–38] MOSFETs,[39–43] as well as p–n diodes,[44–47] their potential in bipolar junction transistors remains entirely unexplored. To the best of our knowledge, no experimental or simulation study on a functional β-Ga_2O_3/GaN HBT has been reported to date. Here, we report the first comprehensive simulation-based demonstration of an n-β-Ga_2O_3/p-GaN/n-GaN HBT, incorporating realistic interfacial defects and compensation effects to provide a physically grounded evaluation of its feasibility, performance, thermal reliability, and optimization strategies under practical defect considerations.

2 Structure and mechanism

The schematic of the simulated HBT structure consists of an n-β-Ga_2O_3 emitter layer with a thickness of 0.15 μm and a doping concentration of $N_D = 2.0 \times 10^{17}$ cm^{-3}, a p-GaN base layer with a thickness of 0.05 μm and $N_A = 2.0 \times 10^{18}$ cm^{-3}, an n-GaN collector layer with a thickness of 0.55 μm and $N_D = 5.0 \times 10^{16}$ cm^{-3}, and an n-GaN subcollector layer with a thickness of 0.15 μm and $N_D = 2.0 \times 10^{17}$ cm^{-3}, as illustrated in Fig. 1. Due to the lateral symmetry of the device structure, only half of the HBT was simulated in the TCAD environment with appropriate symmetry boundary conditions. The full cross-sectional structure is shown in Fig. 1 for clarity. The emitter contact is placed on top of the n-Ga_2O_3 emitter layer to form an ohmic contact, while the base contact is located on the p-GaN base layer. The collector contact is formed on the backside of the n-GaN subcollector layer, also establishing an ohmic contact. The structure, thicknesses, and doping concentrations of the emitter, base, and collector layers in the proposed HBT design are based on those used in InGaP/GaAs heterojunction phototransistors previously fabricated by our group, as reported in ref. 48–50. The key physical models and material parameters used in the simulation, as well as the calibration of model parameters using experimental data, have been described in detail elsewhere.[51,52] In this study, a baseline HBT, referred to as the bulk-trap-only HBT (B-HBT), incorporating key defect-related effects such as deep-level electron traps in the Ga_2O_3 layer, was first established to enhance the accuracy of the simulations. These traps, located at E_C −0.6 eV, E_C −0.75 eV, and E_C −1.05 eV, correspond to the E1, E2, and E3 levels identified in bulk and epitaxial β-Ga_2O_3 films,[53–58] and were included to model carrier trapping and recombination effects more accurately, thereby enhancing the realism of the simulation. To account for experimentally observed non-idealities, a full-trap HBT model, referred to as the F-HBT, was developed. In this case, to simulate the compensation effects induced by oxygen diffusion from the Ga_2O_3 into the p-GaN base, additional defect mechanisms were incorporated in the p-GaN layer: a shallow donor-like trap representing oxygen substituting nitrogen (O_N, E_C −0.03 eV)[59–62] and the dominant shallow acceptor (E_V +0.225 eV) commonly observed in GaN, which is enhanced by oxygen doping and is likely related to a V_{Ga}–O–H complex.[63,64] At the Ga_2O_3/GaN interface, an interface trap density (D_{it}) was introduced to emulate interface defects. A value of $D_{it} \approx 1.0 \times 10^{12}$ eV^{-1} cm^{-2} was used in our simulation. Although Qian Feng *et al.* reported even higher D_{it} values (2.3–5.3 × 10^{13} eV^{-1} cm^{-2}) for mechanically exfoliated β-Ga_2O_3/GaN interfaces,[65] using these values resulted in a complete loss of transistor action in our simulations. Therefore, a reduced D_{it} level was employed to ensure both numerical convergence and preservation of transistor behavior, while still reflecting the experimentally observed interfacial degradation. In addition, polarization-induced charges were enabled with a scaling factor to capture the effect of polarization mismatch and strain relaxation at the monoclinic β-Ga_2O_3/hexagonal GaN interface.[66] This comprehensive trap and interface model (F-HBT) provides a physically grounded description of bulk and interfacial recombination pathways and allows a more rigorous assessment of the degradation mechanisms in Ga_2O_3/GaN HBTs. The modeling assumptions employed in the F-HBT model are not merely hypothetical but are substantiated by experimental findings reported in the literature.[66] In particular, structural and chemical characterizations of β-Ga_2O_3/GaN heterostructures have consistently revealed interfacial traps, strain-induced dislocations, and oxygen-related defect formation, which provide the experimental basis for the adopted full-trap HBT model. Recent experimental characterizations have revealed that the β-Ga_2O_3/GaN heterointerface is far from ideal and strongly influences device performance. High-resolution TEM analyses provide clear evidence of non-abrupt junctions and interfacial defects. For example, Zhang *et al.*[67] observed that β-Ga_2O_3 films grown on GaN substrates form a fuzzy transition layer of 3–4 atomic planes at the interface due to atomic reconfiguration, rather

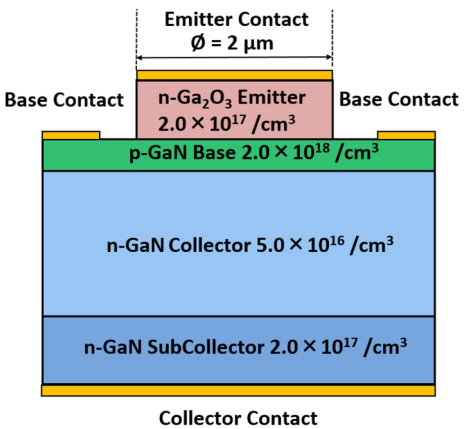

Fig. 1 Cross-sectional schematic of the Ga_2O_3/GaN HBT. Only half of the structure was used for simulation due to symmetry, but the full structure is illustrated here.

than a sharp boundary. Similarly, Seo *et al.*[68] reported that grain boundaries and defect clusters originating from the Ga_2O_3/GaN junction propagate into the overgrown β-Ga_2O_3 layer, confirming the presence of interfacial defect networks. Structural characterizations further highlight the role of lattice mismatch and strain. XRD measurements indicate that GaN grown on β-Ga_2O_3 experiences a lattice mismatch of ~4.7%, resulting in a threading dislocation density (TDD) of ~4.0×10^7 cm^{-2}.[69] Complementary Raman spectroscopy analyses demonstrated a red-shift of the E_2 (high) phonon mode relative to bulk GaN, corresponding to compressive strain of 0.26 GPa in planar GaN/β-Ga_2O_3 LEDs and 0.07 GPa in nanorod structures.[31] These results confirm that both dislocations and residual strain are inevitable at the heterointerface. Chemical analyses also point to interfacial reactions and defect formation. Pre-annealing of GaN substrates prior to β-Ga_2O_3 growth has been shown to substitute N atoms with O atoms, producing a GaN_xO_y interfacial layer.[67] This observation directly supports the formation of O_N-related defects that compensate acceptors in the GaN base. In addition to ON-related compensation, the use of Mg-doped GaN substrates introduces a further risk associated with oxygen incorporation. Pankove *et al.*[70] demonstrated that Mg and O co-doping leads to the formation of Mg–O complexes ('molecular doping'), which effectively scavenge oxygen donors and render the material highly insulating. Such complexes would further reduce the effective hole concentration and thereby hinder hole injection at the Ga_2O_3/GaN interface. These characterizations consistently demonstrate that the β-Ga_2O_3/GaN heterointerface suffers from non-abrupt transitions, strain-induced dislocations, and oxygen-related defect formation.

3 Results and discussion

3.1 Electrical characteristics

Fig. 2 presents the Gummel plots of the simulated Ga_2O_3/GaN B-HBT and F-HBT, showing the base current (I_B) and collector current (I_C) as functions of the base–emitter voltage (V_{BE}) on a logarithmic scale, with the base–collector voltage (V_{BC}) fixed at 0 V. A distinct onset of current amplification is observed when V_{BE} exceeds 2.7 V, marking the turn-on of transistor operation. This relatively high turn-on voltage is consistent with the wide bandgap nature of the n-Ga_2O_3/p-GaN heterojunction and validates the band alignment in the simulation. When bulk traps in Ga_2O_3 as well as comprehensive interfacial effects at the Ga_2O_3/GaN junction are included, the Gummel characteristics exhibit noticeable changes compared with the bulk-trap-only case. In particular, I_C decreases slightly while I_B increases, due to enhanced recombination and carrier capture introduced by defect-related mechanisms at the heterojunction (*e.g.*, interface states, atomic mixing, and non-ideal band profiles). Furthermore, oxygen diffusion from n-Ga_2O_3 emitter into the p-GaN base can generate compensating defects, lowering the effective hole concentration and injection efficiency. As a result, the DC current gain ($\beta_{DC} = I_C/I_B$) of the F-HBT remains in the approximate range of 12–18. This trend is physically reasonable and consistent with experimental reports that interfacial degradation strongly limits the gain of GaN-based HBTs.[71–73] The exponential dependence of I_C and I_B, the clear separation between collector and base currents, and the persistence of current amplification even in the presence of realistic defect modeling confirm that the proposed Ga_2O_3/GaN structure exhibits genuine heterojunction bipolar transistor behavior. Our simulations highlight both the intrinsic performance potential and the limitations imposed by non-ideal interfaces and traps, thereby validating the feasibility of the n-type β-Ga_2O_3 emitter/p-type GaN base/n-type GaN collector structure for future high-power HBT applications.

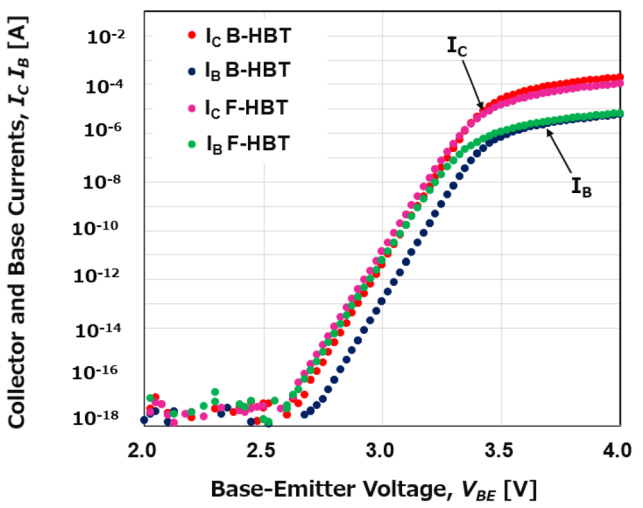

Fig. 2 Room-temperature Gummel plots of the B-HBT and F-HBT with collector–base voltage $V_{CB} = 0$ V.

The room-temperature common-emitter *I–V* characteristics of the simulated Ga_2O_3/GaN B-HBT and F-HBT are presented in Fig. 3. The base current (I_B) was swept from 5 μA to 25 μA in steps of 5 μA, while the collector–emitter voltage (V_{CE}) was varied from 0 to 10 V for each I_B. An offset voltage ($V_{CE,offset}$) as low as 0.25 V was observed, which is substantially lower than that of typical AlGaN/GaN HBTs (2 V)[73–75] and comparable to InGaN/GaN HBTs (0.3 V).[76,77] The DC current gain (β_{DC}) was extracted from the output curves in Fig. 3 and plotted as a function of I_B in Fig. 4. With increasing I_B, the collector current (I_C) rises proportionally, indicating effective current modulation and forward-active transistor operation. Each output curve exhibits a steep increase in I_C at low V_{CE}, followed by a well-defined saturation region where I_C remains nearly constant with further increases in V_{CE}. This behavior reflects efficient carrier injection across the n-Ga_2O_3/p-GaN emitter–base junction and minimal base-width modulation (Early effect), highlighting excellent device stability and linearity—key requirements for high-frequency and high-power applications. Furthermore, as shown in Fig. 3, the collector current I_C of the F-HBT is lower than that of the B-HBT, and the F-HBT also exhibits a slight upward shift in the knee voltage. In addition, the saturation region of the F-HBT becomes flatter, indicating a smaller Early effect. The degradation in the F-HBT is attributed to additional recombination pathways introduced at the Ga_2O_3/GaN boundary, together with parasitic resistances and

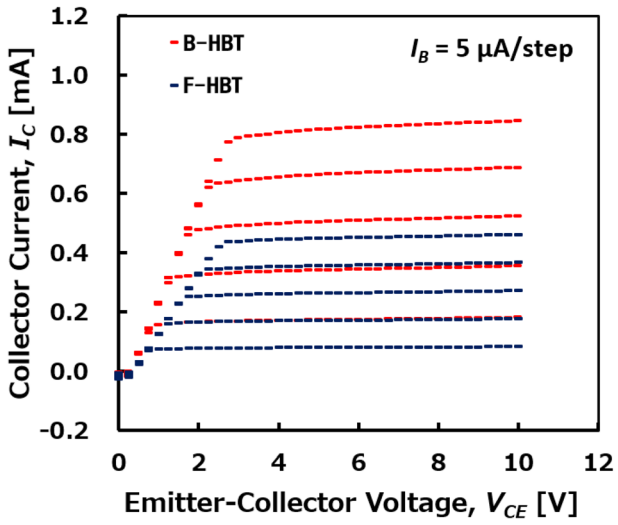

Fig. 3 Room-temperature common-emitter *I–V* characteristics of the B-HBT and F-HBT for base currents varying from 5 μA to 25 μA in steps of 5 μA.

oxygen-related compensation in the p-GaN base. These trends are consistent with the Gummel plots shown in Fig. 2, further confirming the physical validity of the defect-inclusive model. Despite the incorporation of all relevant traps, the collector current I_C of the F-HBT still increases with V_{CE} and then saturates, confirming effective current modulation and forward-active operation similar to that of the B-HBT.

The specific on-resistance ($R_{on,sp}$) of the B-HBT and F-HBT was determined to be 0.19 mΩ cm^2 and 0.35 mΩ cm^2, respectively, at $V_{CE} = 5$ V with $I_B = 25$ μA and $I_C = 815$ μA for the B-HBT and $I_C = 450$ μA for the F-HBT. These values were calculated based on a circular emitter region with a radius of 1.0 μm, corresponding to high collector current densities (J_C) of 26 kA cm^{-2} and 14.3 kA cm^{-2}, respectively. As shown in Fig. 4, the DC current gain of the B-HBT remains nearly constant or exhibits a slight decline as I_B increases, reflecting an almost idealized response dominated by bulk traps. In contrast, the F-HBT demonstrates a slight increase in β_{DC} with I_B, which is consistent with our earlier experimental observations in InGaP/GaAs heterojunction phototransistors (HPTs).[48–50] In those devices, β_{DC} also increased with I_B because recombination at the emitter perimeter and heterointerface became relatively less significant at higher injection levels, while the diffusion current dominated. A similar mechanism can be used to explain the behavior of the F-HBT: at low I_B, interface and compensation defects dominate recombination, suppressing β_{DC}, whereas at higher I_B these defects are partially saturated, allowing the diffusion current to prevail, thereby improving injection efficiency and slightly enhancing β_{DC}. Specifically, β_{DC} in the B-HBT decreases modestly from 35.4 at $I_B = 5$ μA to 33.4 at $I_B = 25$ μA (5.7% reduction), whereas in the F-HBT it increases from 16.5 to 18.3 (11% enhancement) over the same bias range at $V_{CE} = 8.0$ V. This difference clearly demonstrates that the full-trap model more realistically captures the bias-dependent behavior observed in practical heterojunction devices.

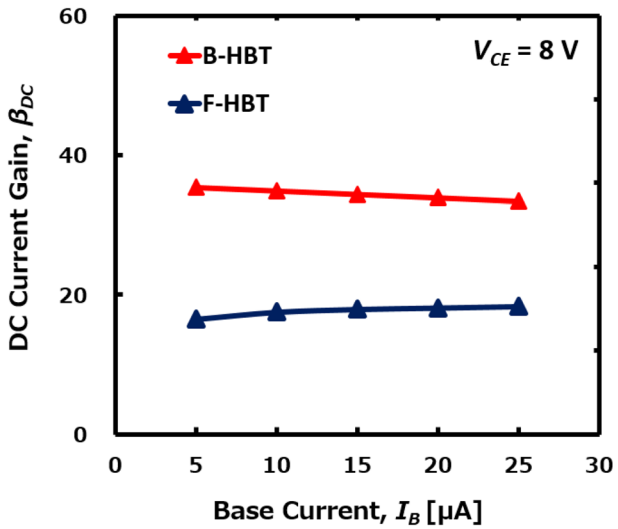

Fig. 4 Room-temperature DC current gains of the B-HBT and F-HBT for various base currents.

As shown in Fig. 4, the DC current gain (β_{DC}) of the F-HBT remains in the range of 16–18 for base currents (I_B) between 5 and 25 μA, which is more than twice lower than that of the B-HBT. The reduced β_{DC} is associated with defect-assisted recombination at the Ga_2O_3/GaN boundary, originating from lattice mismatch, interdiffusion, and associated band-edge distortions. These defects act as strong recombination centers in the depletion region of the emitter–base junction, thereby increasing the base current and reducing the DC current gain. A similar mechanism was also observed in our previous studies on InGaP/GaAs HPTs, where defect generation at the heterointerface and at the emitter perimeter enhanced recombination and degraded both current gain and photoresponse. In the Ga_2O_3/GaN system, additional parasitic resistances at the heterointerface and compensating defects in the p-GaN base induced by oxygen diffusion further reduce the hole concentration and emitter injection efficiency. These findings are consistent with experimentally observed trends in GaN-based HBTs, providing a credible explanation for the performance limitations and highlighting that interface quality, defect passivation, and device design strategies are crucial to realize high-performance β-Ga_2O_3/GaN HBTs.

The collector current (I_C) as a function of the reverse-biased collector–base voltage (V_{CB}), with both the base and emitter grounded, was simulated to determine the breakdown voltage of the HBT, as shown in Fig. 5. V_{CB} was swept from 0 V to 200 V to evaluate the collector–base breakdown behavior (BV_{CBO}). For both the B-HBT and F-HBT, I_C remains nearly zero until a sharp increase occurs at approximately 120 V, which is identified as the collector–base breakdown voltage (BV_{CBO}) of the Ga_2O_3/GaN HBT structure. However, the collector current of the F-HBT is slightly suppressed beyond breakdown compared to that of the B-HBT, reflecting the additional influence of interface-related defects and compensation effects. The transistor's power figure of merit (PFOM) for the B-HBT and F-HBT, defined as $BV_{CBO}^2/R_{on,sp}$, was calculated to be 74.8 MW cm^{-2} and 41.3 MW

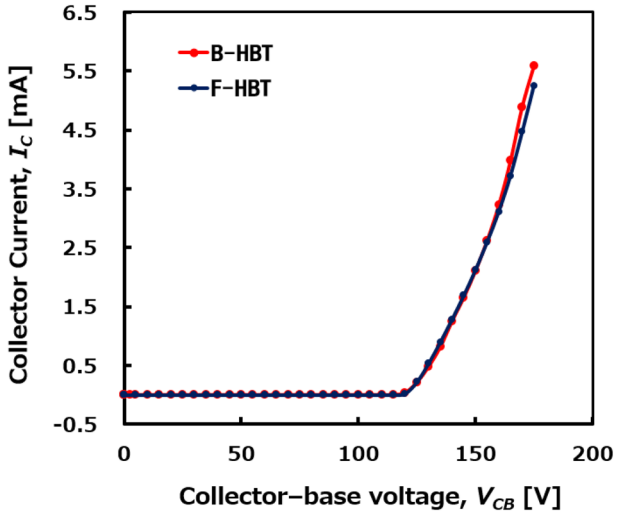

Fig. 5 Simulated collector current as a function of the reverse-biased collector–base voltage (V_{CB}) at room temperature, with both the base and emitter grounded. The sharp increase in I_C at approximately 120 V indicates the collector–base breakdown voltage (BV_{CBO}) of the Ga_2O_3/GaN HBT.

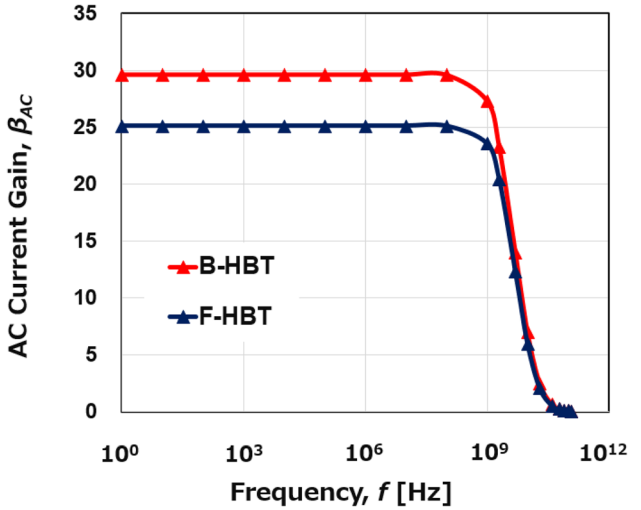

Fig. 6 Simulated AC current gain (β_{AC}) of the B-HBT and F-HBT as a function of frequency. The cutoff frequency (f_T) is defined as the frequency at which the current gain drops to unity.

cm^{-2}, respectively. The high breakdown voltage, primarily governed by the intrinsic wide-bandgap nature of Ga_2O_3 and GaN together with the engineered heterojunction profile, demonstrates the robust reverse-blocking capability of the proposed HBT structure. Furthermore, the high PFOM confirms a favorable trade-off between breakdown performance and conduction loss, indicating strong potential for high-voltage power switching applications.

In addition to their application in high-voltage power switching, HBTs are also widely used in RF and high-speed switching circuits. Therefore, the high-frequency performance of the proposed Ga_2O_3/GaN HBT was evaluated by extracting the cutoff frequency (f_T), defined as the frequency at which the short-circuit current gain drops to unity. As seen in Fig. 6, the AC current gain (β_{AC}) remains nearly constant at 29.6 up to frequencies near 10^9 Hz and then decreases rapidly, with f_T determined to be approximately 35 GHz for the B-HBT. By contrast, the F-HBT exhibits a lower low-frequency β_{AC} (25.1) compared to the B-HBT (29.6), with the roll-off occurring at a lower frequency. The cutoff frequency f_T of the F-HBT is reduced to approximately 30 GHz, which is 14.3% lower than that of the B-HBT. The reduction in f_T for the F-HBT is attributed to carrier recombination and trapping at the heterojunction, which increase the effective base transit time and parasitic resistances, thereby degrading the high-frequency response. Despite this reduction, both the B-HBT and F-HBT maintain effective operation at high frequencies. The simulated f_T values are consistent with the device's structural parameters, including a short base width of 50 nm, moderate emitter and collector doping levels, and optimized GaN/β-Ga_2O_3 heterojunction alignment. Although β-Ga_2O_3 has inherently low electron mobility, the relatively thin base region and the high carrier saturation velocity in GaN help reduce the carrier transit time, thereby enhancing f_T. Moreover, the combination of GaN and β-Ga_2O_3, two materials with wide bandgaps and high breakdown fields, enables robust high-frequency operation without premature breakdown. Compared to other wide-bandgap devices, the proposed β-Ga_2O_3/GaN HBT exhibits competitive high-frequency performance.[78,79] The B-HBT achieves an f_T of 35 GHz, serving as an upper bound under bulk-trap-only conditions, while the F-HBT maintains an f_T of 30 GHz, comparable to reported values for β-Ga_2O_3 MOSFETs (27 GHz)[79] and significantly exceeding that of AlGaN/GaN HBTs (4.05 GHz).[78] Our simulations show that even under realistic full-trap conditions, the β-Ga_2O_3/GaN HBT sustains frequency performance on par with or better than established wide-bandgap technologies, while simultaneously providing superior breakdown capability. Furthermore, to the best of our knowledge, this study presents the first demonstration of a functional HBT based on the Ga_2O_3/GaN material system, even though Ga_2O_3/GaN heterojunctions have been extensively investigated for unipolar and optoelectronic devices such as p–n diodes, HEMTs, MOSFETs, and LEDs, as summarized in Table 1. By employing a p-GaN base to circumvent the long-standing challenge of p-type doping in β-Ga_2O_3, our work not only opens a new avenue for the development of Ga_2O_3-based bipolar devices but also contributes a novel device architecture to the wide-bandgap semiconductor field.

3.2 Temperature-dependent electrical characteristics of Ga_2O_3/GaN HBTs

For power electronics applications, particularly in power switching environments, the β-Ga_2O_3/GaN HBT must be capable of operating at elevated temperatures. As previously discussed, the combination of an ultra-wide bandgap β-Ga_2O_3 emitter with a high-performance p-GaN base and n-GaN collector provides a promising material platform, enabling the proposed β-Ga_2O_3/GaN HBT to achieve high performance. At

Table 1 Comparison of the current work with previously reported Ga_2O_3/GaN devices

Device	Key material layers	Primary function	Novelty	Reference
p–n diode	Ga_2O_3 (n-type), GaN (p-type)	High-performance rectifiers and power diodes with high breakdown voltage, low switching loss, and scalability for high-frequency power electronics	(i) β-Ga_2O_3/GaN Junction Barrier Schottky diode (JBSD) with high breakdown and fast switching; (ii) transfer-printed β-Ga_2O_3 nanomembranes for large-area devices; (iii) improved termination designs to maximize breakdown	44–47
HEMT	Ga_2O_3 layers integrated with GaN (heterojunction or gate oxide)	Fabrication of high-performance, normally-off, reliable HEMTs/MOSHEMTs for high-power and high-frequency applications	Using β-Ga_2O_3 as a gate dielectric/stack to enhance 2DEG density, raise threshold voltage, suppress leakage, and improve thermal/noise performance	25 and 32–38
MOSFET	β-Ga_2O_3 channel (grown by mist chemical vapor deposition (mist-CVD) on GaN substrates) and Ga_2O_3 gate dielectric (formed by photo-enhanced chemical (PEC) oxidation of GaN nanowires (NWs))	High-power, reliable, low-cost MOSFETs suitable for high-voltage power electronics	(i) PEC oxidation for Ga_2O_3/GaN hybrid NW MOSFETs; (ii) mist-CVD instead of MOCVD/MBE for cost-effective, high-performance β-Ga_2O_3 MOSFETs; (iii) very high breakdown voltage without complex structures	39–43
Photodetector	β-Ga_2O_3/GaN heterojunctions	Dual-mode, deep-UV high-selectivity, and high-resolution narrow-band UV photodetection	Bias-controlled dual-mode, dual-band high-responsivity, and ultranarrow spectral response	26–28
LED	GaN/InGaN LEDs on β-Ga_2O_3 substrates or with embedded patterned/nanorod Ga_2O_3 structures	High-efficiency GaN-based LEDs with improved light output, internal quantum efficiency, and photon extraction	First green LED on β-Ga_2O_3; Ga_2O_3 patterning and nanorods enhance light output power (LOP), internal quantum efficiency (IQE), and light extraction efficiency (LEE), while reducing strain and quantum-confined Stark effect (QCSE)	29–31
This work	n-β-Ga_2O_3 emitter/p-GaN base/n-GaN collector	A high-gain, high-frequency, high-breakdown transistor for next-generation power electronics and RF switching	First demonstration of a functional Ga_2O_3/GaN HBT *via* simulation, overcoming the lack of p-type β-Ga_2O_3, with realistic trap/interface modeling and structural optimization	

room temperature, the B-HBT delivered a high collector current density (J_C) of 26 kA cm^{-2} at a base current of 25 μA, corresponding to a power figure of merit (PFOM) of 74.8 MW cm^{-2} and a low specific on-resistance ($R_{on,sp}$) of 0.19 mΩ cm^2. In comparison, the F-HBT exhibited a J_C of 14.3 kA cm^{-2}, yielding a PFOM of 41.3 MW cm^{-2} and a $R_{on,sp}$ of 0.35 mΩ cm^2. These results demonstrate strong competitiveness compared to conventional GaN-based HBTs.[76–78] However, to assess the practical applicability of the device, it is essential to investigate the temperature dependence of key parameters such as collector current, current gain, specific on-resistance, and PFOM, in addition to performance under ideal conditions.

The temperature-dependent performance of the Ga_2O_3/GaN HBT was systematically investigated over the range of 300 K to 460 K, as shown in Fig. 7–11. Fig. 7 compares the common-emitter *I–V* characteristics of the Ga_2O_3/GaN HBT at 300 K and 460 K with a base current step of 5 μA. A noticeable degradation in collector current is observed at 460 K compared to 300 K, especially at higher base current levels, indicating deteriorated carrier transport at elevated temperatures. However, at both temperatures, the *I–V* characteristics exhibit a distinct forward-active behavior, with a sharp increase in collector current (I_C) at low V_{CE} followed by well-defined saturation regions. In addition, an increased offset voltage and reduced flatness in the saturation region at 460 K indicate mild base-width modulation and enhanced thermal effects. The B-HBT delivers higher I_C at both temperatures, whereas the F-HBT exhibits lower absolute I_C and poorer high-temperature

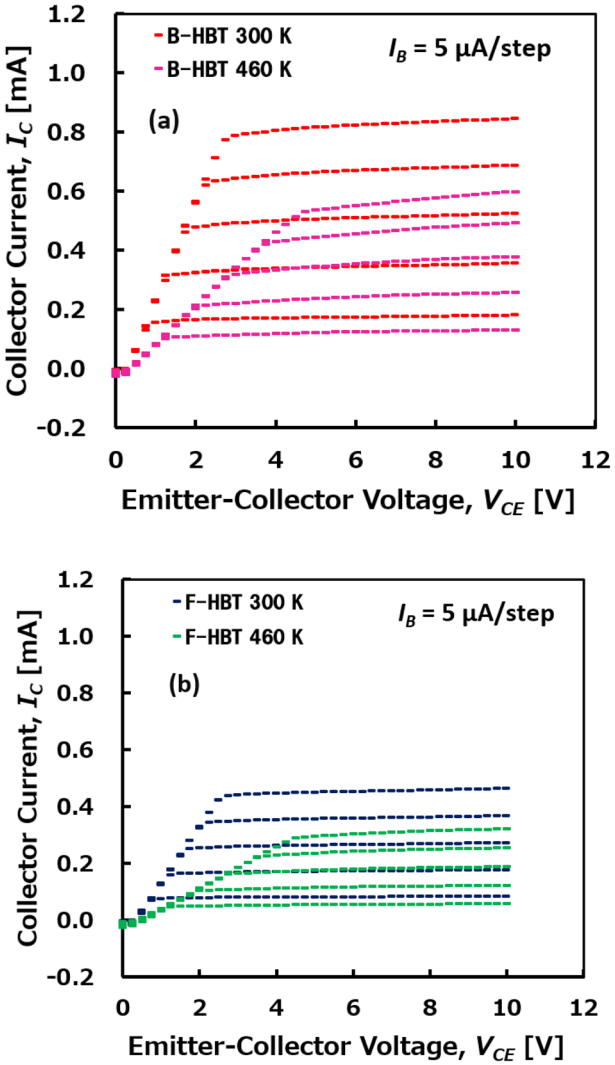

Fig. 7 Common-emitter I–V characteristics of β-Ga_2O_3/GaN HBTs at 300 K and 460 K with a base-current step of 5 μA: (a) B-HBT (bulk-trap-only model) and (b) F-HBT (full-trap model).

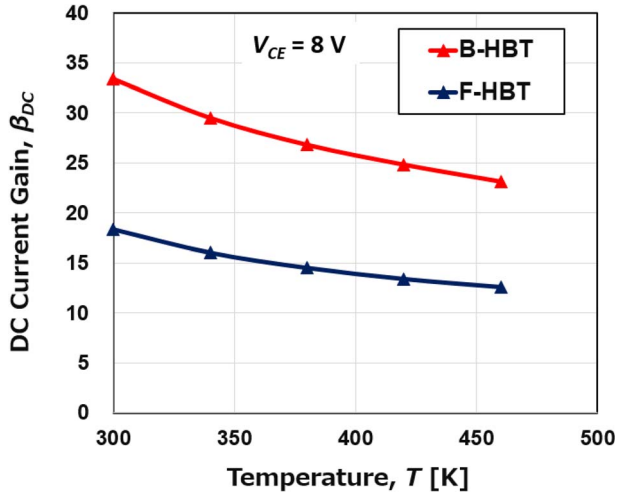

Fig. 8 Temperature dependence of the DC current gain (β_{DC}) of the B-HBT and F-HBT at a fixed base current of 25 μA.

performance, reflecting the impact of heterojunction-related non-idealities and compensation effects in the p-GaN base. Consequently, both devices exhibit reduced DC current gain (β_{DC}) with temperature: the B-HBT decreases from 33.4 at 300 K to 23.1 at 460 K (31% reduction), while the F-HBT falls from 18.3 to 12.6 (31% reduction). Although the fractional degradation with temperature is similar, the F-HBT consistently operates with substantially lower absolute gain across the examined range, emphasizing the critical role of interface quality and defect control for reliable high-temperature Ga_2O_3/GaN HBT operation. The degradation in β_{DC} with increasing temperature is primarily attributed to enhanced carrier recombination in the base region and reduced carrier mobility at elevated temperatures, which together lower the emitter-to-base injection efficiency. In addition, higher temperatures facilitate hole back-injection across the emitter–base junction, further reducing injection efficiency. Moreover, the minority carrier lifetime decreases with temperature due to thermally activated deep-level traps and enhanced non-radiative recombination in both p-GaN and n-β-Ga_2O_3. The shortened lifetime accelerates recombination, decreases the base transport factor, and thereby further degrades the overall current gain. Compared with the B-HBT, the F-HBT suffers from stronger degradation because junction imperfections act as recombination centers and increase parasitic resistance, while compensating defects in the p-GaN base lower the effective hole concentration and weaken emitter injection efficiency.

Simultaneously, Fig. 9 and 10 show a consistent thermal response in both devices: as the temperature increases from 300 to 460 K, the specific on-resistance ($R_{on,sp}$) rises monotonically, accompanied by a decline in the power figure of merit (PFOM). For the B-HBT, $R_{on,sp}$ increases from 0.19 to 0.29 mΩ cm^2 while PFOM drops from 74.8 to 49.2 MW cm^{-2}. Likewise, the F-HBT shows a rise in $R_{on,sp}$ from 0.35 to 0.50 mΩ cm^2 and a reduction in PFOM from 41.3 to 28.9 MW cm^{-2}. This degradation is

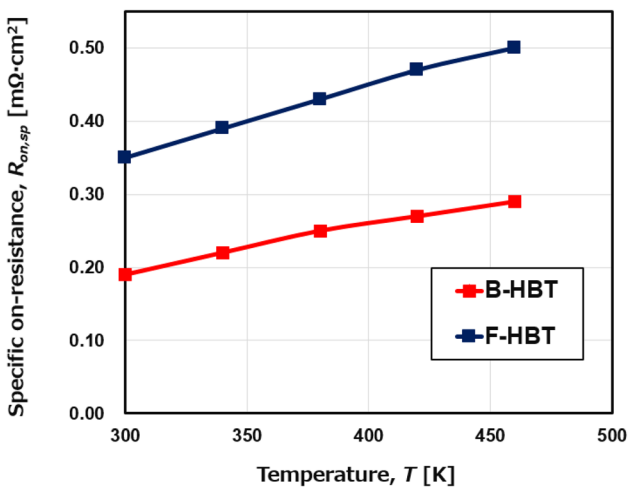

Fig. 9 Temperature dependence of the specific on-resistance ($R_{on,sp}$) of the B-HBT and F-HBT at a fixed base current of 25 μA.

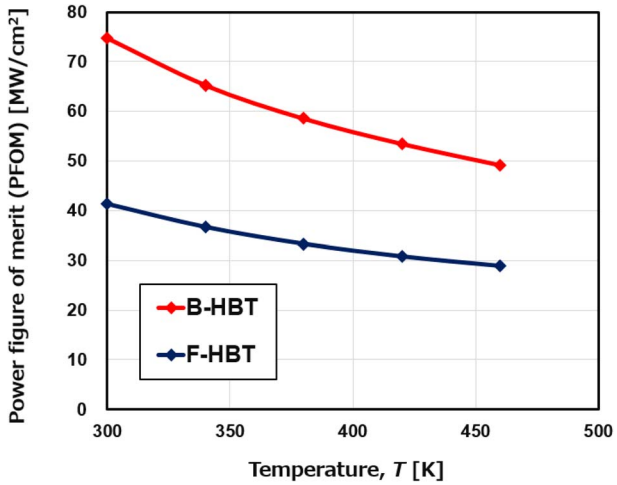

Fig. 10 Temperature dependence of the power figure of merit (PFOM) of the B-HBT and F-HBT at a fixed base current of 25 μA.

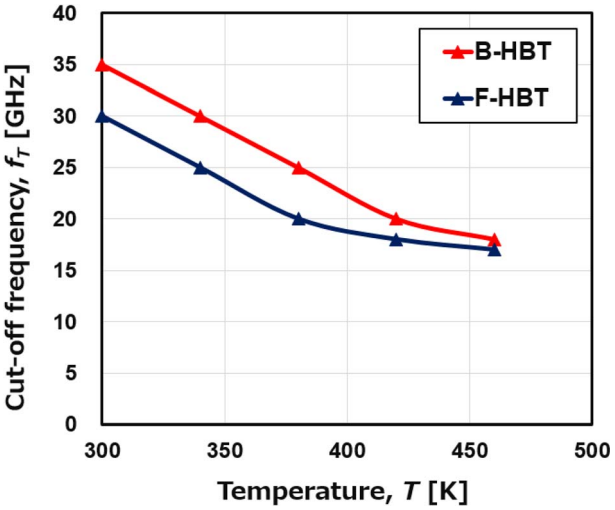

Fig. 11 Temperature dependence of the cutoff frequency (f_T) of the B-HBT and F-HBT.

attributed to thermally reduced electron mobility in the β-Ga_2O_3 emitter and drift regions. Importantly, the collector–base breakdown voltage (BV_{CBO}) remains nearly constant at 120 V, confirming that the PFOM loss originates mainly from resistance increases rather than breakdown changes. Elevated resistance in the collector region also produces a larger voltage drop under fixed bias (V_C), thereby reducing the effective junction voltage and lowering the collector current (I_C). The combined effect of higher $R_{on,sp}$ and suppressed I_C results in substantial PFOM degradation. This trend is corroborated by the output characteristics in Fig. 7, which show significantly higher I_C at 300 K compared to 460 K for the same collector–emitter voltage (V_{CE}). The consistency between the *I–V* characteristics and PFOM decline highlights the thermal sensitivity of the device performance. This analysis demonstrates that although the proposed HBT structure maintains stable operation at elevated temperatures, both current gain and power efficiency are subject to significant thermal degradation, which must be carefully addressed in the design of high-temperature power and RF devices.

Heterojunction bipolar transistors (HBTs) are commonly used in practical RF and power switching applications, where they often operate under elevated thermal conditions. Therefore, evaluating the temperature dependence of the cutoff frequency (f_T) is essential for understanding the high-frequency reliability and performance limits of the proposed Ga_2O_3/GaN HBT. As seen in Fig. 11, f_T decreases monotonically with temperature for both device variants. For the B-HBT, f_T falls from 35 to 18 GHz as *T* increases from 300 to 460 K, whereas the F-HBT decreases from 30 to 17 GHz. The full-trap device consistently exhibits lower f_T due to reduced transconductance and higher parasitic resistance/capacitance from interfacial defects; however, the gap between the two devices narrows at elevated temperatures where phonon-limited mobility dominates. This degradation is primarily driven by enhanced phonon scattering in the β-Ga_2O_3 emitter and GaN collector, which reduces carrier mobility, increases base transit time, and elevates diffusion capacitance and base resistance. Despite this, the proposed HBT maintains a competitive f_T across the investigated range. The wide bandgap of n-β-Ga_2O_3 ensures a high breakdown voltage, while the p-GaN base provides thermal stability along with efficient minority-carrier injection and fast switching. These combined attributes highlight the promise of β-Ga_2O_3/GaN HBTs for high-temperature, high-frequency power and RF applications.

3.3 Effect of base and collector thickness on the electrical performance of Ga_2O_3/GaN HBTs

The performance of heterojunction bipolar transistors (HBTs) can be enhanced by optimizing the base and collector thicknesses, specifically by balancing the trade-offs between current gain, breakdown voltage, and conduction loss. To clarify these effects, the electrical performance of the proposed β-Ga_2O_3/GaN HBT was evaluated as a function of base and collector thickness. First, all device parameters were kept constant while the base thickness (t_B) was varied from 0.05 μm to 0.15 μm. For each t_B, key parameters such as current gain, breakdown voltage, specific on-resistance ($R_{on,sp}$), and power figure of merit (PFOM) were extracted and analyzed.

Fig. 12(a) presents the dependence of DC current gain (β_{DC}) and power figure of merit (PFOM) on base thickness (t_B). As t_B increases from 0.05 μm to 0.15 μm, β_{DC} for both the B-HBT and F-HBT decreases significantly due to enhanced carrier recombination and prolonged transit time through the thicker base region. In contrast, PFOM generally increases with t_B, primarily driven by the substantial enhancement in breakdown voltage, which outweighs the concurrent increase in specific on-resistance ($R_{on,sp}$), as shown in Fig. 12(b). Across the entire thickness range, the F-HBT exhibits lower β_{DC} and PFOM than the B-HBT, consistent with additional interfacial traps and parasitic resistances at the β-Ga_2O_3/GaN junction that hinder carrier transport. As seen in Fig. 12(b), the breakdown voltage of both devices increases markedly with t_B, since a thicker base

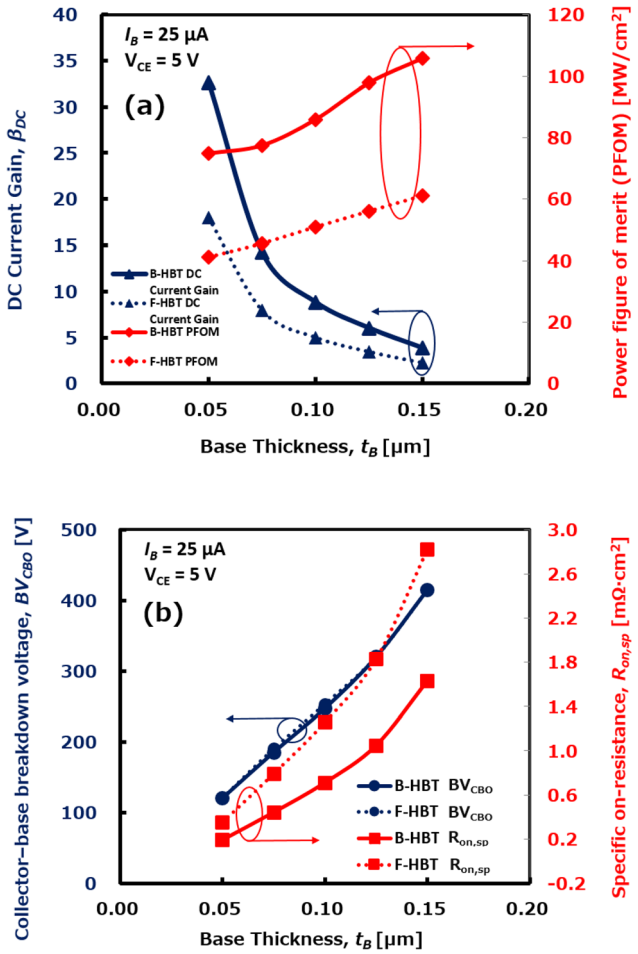

Fig. 12 Dependence of (a) DC current gain (β_{DC}) and power figure of merit (PFOM), and (b) collector–base breakdown voltage (BV_{CBO}) and specific on-resistance ($R_{on,sp}$) on base thickness (t_B) for the B-HBT and F-HBT, evaluated at $I_B = 25$ μA and $V_{CE} = 5$ V.

broadens the depletion region, thereby improving electric field distribution and enhancing voltage blocking capability. Meanwhile, $R_{on,sp}$ exhibits a noticeable increase with t_B due to the longer transport path and higher series resistance in the base/collector stack. Adjusting the base thickness proves to be an effective strategy for balancing switching efficiency and voltage robustness in Ga_2O_3/GaN HBTs. The base thickness (t_B) critically influences the overall device performance. A thinner base significantly enhances the DC current gain (β_{DC}) by reducing carrier transit time and minimizing recombination within the base region, which are essential factors for high-gain amplification and RF operation. However, a thin base limits the breakdown voltage and PFOM due to a narrower depletion region and weaker electric field control. In contrast, increasing the base thickness substantially improves breakdown voltage and PFOM, although it leads to a degradation in β_{DC}. Therefore, an optimized base thickness offers a favorable trade-off. It provides sufficient current gain for efficient switching while maintaining high power performance and voltage robustness, which are critical for the practical implementation of Ga_2O_3/GaN HBTs in high-voltage and high-frequency power applications.

Next, the effect of collector thickness (t_C) on device performance was investigated by varying t_C from 0.5 μm to 2.0 μm while keeping all other HBT parameters constant. The dependence of key performance metrics on collector thickness was systematically analyzed, and the corresponding simulation results are presented in Fig. 13. As illustrated in Fig. 13(a), the DC current gain (β_{DC}) of both B-HBT and F-HBT remains nearly constant, at approximately 32 for the B-HBT and 18 for the F-HBT, across the entire range of collector thickness (t_C). This suggests that increasing the collector thickness does not significantly influence carrier injection efficiency or recombination within the base, as β_{DC} is primarily determined by the emitter–base junction characteristics. In contrast, the power figure of merit (PFOM) exhibits a substantial enhancement, rising from 62.9 MW cm^{-2} at $t_C = 0.5$ μm to over 248 MW cm^{-2} at $t_C = 2.0$ μm for the B-HBT, and from 34.7 MW cm^{-2} to over 138 MW cm^{-2} for the F-HBT over the same thickness range. This improvement is mainly due to the increase in breakdown voltage (BV_{CBO}) with thicker collector layers, as shown in Fig. 13(b). A thicker collector enables a wider depletion region

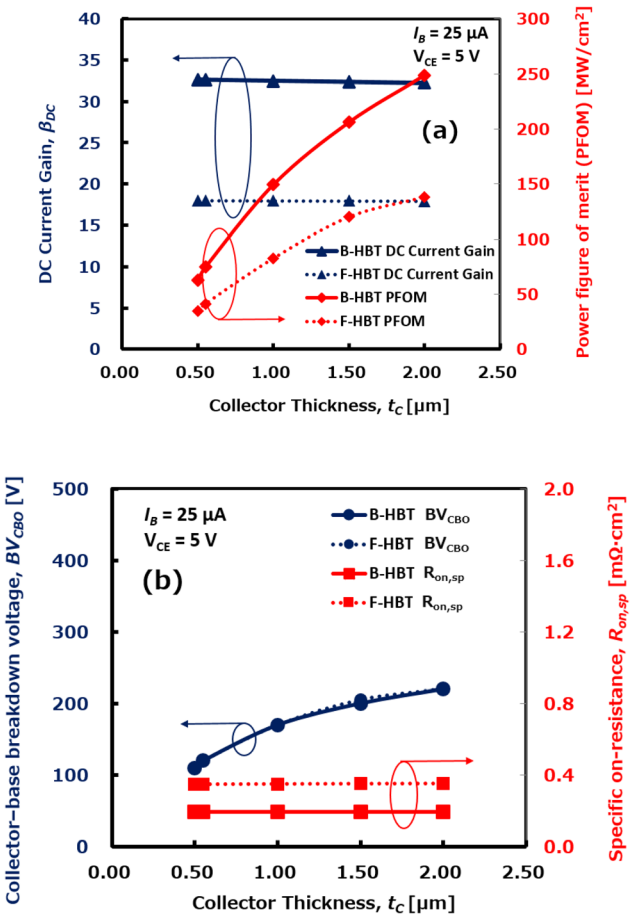

Fig. 13 Dependence of (a) DC current gain (β_{DC}) and power figure of merit (PFOM), and (b) collector–base breakdown voltage (BV_{CBO}) and specific on-resistance ($R_{on,sp}$) on collector thickness (t_C) for the B-HBT and F-HBT, evaluated at $I_B = 25$ μA and $V_{CE} = 5$ V.

Table 2 Comparison of the proposed Ga_2O_3/GaN HBT with previously reported wide-bandgap devices

Device structure	DC current gain (β_{DC})	Breakdown voltage (V)	$R_{on,sp}$ (mΩ cm^2)	PFOM (MW cm^{-2})	f_T (GHz)	Year	Reference
Ga_2O_3/GaN HBT (B-HBT)	34.9	120	0.19	74.8	35	2025	This work
Ga_2O_3/GaN HBT (F-HBT)	18.3	120	0.35	41.3	30	2025	This work
Cu_2O/β-Ga_2O_3 HBT	>50	3540–280	—	34.0	—	2023	23
AlGaN/GaN HBT	129	160	0.28	91.0	4.05	2022	78
AlGaN/GaN HBT	25	—	—	—	—	2022	72
AlGaN/GaN HBT	2	—	—	—	—	2016	80
InGaN/GaN HBT	24	105	0.14	~78.7	—	2013	81
GaN/InGaN HBT	>24	>95	—	—	> 5	2011	77
AlGaN/GaN HBT	18	>330	—	—	—	2003	73
GaN/AlGaN HBT	10	—	—	—	—	2000	71
β-Ga_2O_3 MESFET	—	150	—	—	27	2019	79

and a more uniform electric field distribution, thereby enabling significantly higher breakdown voltage. Specifically, BV_{CBO} increases from approximately 110 V to 220 V for both devices as t_C increases. Notably, the specific on-resistance ($R_{on,sp}$) shows only minor variation across the same thickness range, indicating that enhanced thickness does not introduce significant resistance penalties. Although both devices benefit from collector thickening, the F-HBT consistently exhibits a lower DC current gain, which can be attributed to defect-related recombination at the Ga_2O_3/GaN junction arising from interfacial imperfections and structural mismatches. Consequently, the F-HBT also demonstrates a lower PFOM across the entire range, since such interfacial defects raise parasitic resistances. These results demonstrate that optimizing the collector thickness is an effective strategy for enhancing the breakdown strength and power efficiency of Ga_2O_3/GaN HBTs, without compromising DC current gain or $R_{on,sp}$. Furthermore, this approach offers a promising solution for improving the trade-off between high-voltage capability and conduction loss in high-power switching applications.

Our simulations show that both base thickness (t_B) and collector thickness (t_C) play pivotal roles in determining the overall performance of Ga_2O_3/GaN HBTs, although their effects manifest in distinct ways. A thinner base is favorable for applications requiring high gain and fast response, but it compromises breakdown voltage and PFOM. In contrast, increasing the collector thickness exhibits a dominant and beneficial impact on key performance metrics; a thicker collector enhances both breakdown voltage and PFOM without causing significant degradation in β_{DC} or $R_{on,sp}$. This finding is scientifically significant because it reveals a practical and fabrication-compatible approach to improve voltage endurance and switching efficiency without sacrificing current gain. This trade-off between current gain and breakdown performance has long been a challenge in HBT design. Therefore, a structural configuration with a thin base and a moderately thick collector is recommended to achieve optimized performance. This combination supports a favorable balance among DC current gain, power efficiency, and voltage robustness, making it particularly suitable for high-voltage, high-frequency power switching, compact power ICs, and RF front-end modules.

Table 2 provides a comparative overview of the key performance metrics of the proposed Ga_2O_3/GaN HBT in relation to previously reported wide-bandgap devices. As shown in Table 2, experimental AlGaN/GaN HBTs[78] exhibit very high current gain (up to 129) but suffer from limited cutoff frequencies (<5 GHz), whereas InGaN/GaN HBTs[77,81] deliver moderate current gain but relatively low breakdown voltages (~95–105 V). Simulation results of Cu_2O/β-Ga_2O_3 HBTs[23] indicate the potential for high breakdown voltages (>3 kV); however, the narrow bandgap of the p-type base material fundamentally limits their performance. In contrast, the simulated Ga_2O_3/GaN HBT proposed in this work achieves a well-balanced trade-off among current gain, breakdown voltage, PFOM, and frequency response, thereby positioning it as a promising candidate for next-generation power and RF electronic applications. By comparing the characteristics of the B-HBT and F-HBT, it becomes evident that the Ga_2O_3/GaN heterointerface is the primary bottleneck for achieving high-performance HBTs. Our simulations further reveal that only a low density of interface trap ($D_{it} \approx 1.0 \times 10^{12}$ eV^{-1} cm^{-2}) is compatible with transistor operation, whereas the higher trap densities reported experimentally ($2.3–5.3 \times 10^{13}$ eV^{-1} cm^{-2}) would completely suppress device functionality. The feasibility of Ga_2O_3/GaN HBTs therefore hinges on improving interface quality through optimized growth processes, suppression of oxygen diffusion, and advanced strain engineering. It is concluded that stringent interface control is essential as the critical pathway to translate the promising theoretical performance of Ga_2O_3/GaN HBTs into practical applications.

4 Conclusions

In this work, a β-Ga_2O_3/GaN heterojunction bipolar transistor (HBT) featuring an n-type β-Ga_2O_3 emitter, a p-type GaN base, and an n-type GaN collector was designed and simulated to overcome the limitations of β-Ga_2O_3 bipolar devices caused by the absence of reliable p-type doping. Our simulation results confirm, for the first time, that the β-Ga_2O_3/GaN structure can effectively function as a heterojunction bipolar transistor. The proposed device with full consideration of traps achieves a high DC current gain of 18.3 and an ultra-low specific on-resistance

($R_{on,sp}$) of 0.35 mΩ cm^2, resulting from efficient carrier injection across the n-β-Ga_2O_3/p-GaN heterojunction and optimized layer thicknesses. The collector–base breakdown voltage (BV_{CBO}) reaches 120 V, yielding a power figure of merit (PFOM) of 41.3 MW cm^{-2}. A cutoff frequency (f_T) of 30 GHz demonstrates competitive high-frequency performance. Moreover, the device retains stable operation at elevated temperatures up to 460 K, despite predictable degradation in DC current gain and PFOM, primarily due to reduced carrier mobility and increased recombination. Structural optimization further shows that a thin base preserves high gain, while a thicker collector improves PFOM by enhancing breakdown voltage without degrading $R_{on,sp}$ or β_{DC}. These findings highlight the strong potential of the Ga_2O_3/GaN HBT for high-voltage and high-frequency applications, positioning it as a promising candidate to bridge the performance gap between ultra-wide-bandgap oxides and III-nitride semiconductors.

Author contributions

Phuc Hong Than: conceptualization, formal analysis, investigation, methodology, resources, validation, writing – original draft, writing – review & editing; Tho Quang Than: conceptualization, data curation, formal analysis, investigation, methodology, writing – review & editing; and Yasushi Takaki: conceptualization, investigation, formal analysis, resources, writing – review & editing.

Conflicts of interest

The authors declare no conflict of interest.

Data availability

The data that support the findings of this study are available from the corresponding author upon reasonable request.

Acknowledgements

The authors sincerely thank Prof. Cong-Kha Pham from the University of Electro-Communications (UEC), Tokyo, Japan, for his valuable technical advice and support.

References

1 S. J. Pearton, J. Yang, P. H. Cary, F. Ren, J. Kim, M. J. Tadjer and M. A. Mastro, A review of Ga_2O_3 materials, processing, and devices, *Appl. Phys. Rev.*, 2018, **5**(1), 011301.
2 C. Wang, J. Zhang, S. Xu, C. Zhang, Q. Feng, Y. Zhang, J. Ning, S. Zhao, H. Zhou and Y. Hao, Progress in state-of-the-art technologies of Ga_2O_3 devices, *J. Phys. D Appl. Phys.*, 2021, **54**(24), 243001.
3 J. Zhang, J. Shi, D.-C. Qi, L. Chen and K. H. L. Zhang, Recent progress on the electronic structure, defect, and doping properties of Ga_2O_3, *APL Mater.*, 2020, **8**(2), 020906.
4 J. Montes, C. Kopas, H. Chen, X. Huang, T. H. Yang, K. Fu, C. Yang, J. Zhou, X. Qi, H. Fu and Y. Zhao, Deep level transient spectroscopy investigation of ultra-wide bandgap (−201) and (001) β-Ga_2O_3, *J. Appl. Phys.*, 2020, **128**(20), 205701.
5 M. Bosi, P. Mazzolini, L. Seravalli and R. Fornari, Ga_2O_3 polymorphs: Tailoring the epitaxial growth conditions, *J. Mater. Chem. C*, 2020, **8**(32), 10975–10992.
6 H. Aida, K. Nishiguchi, H. Takeda, N. Aota, K. Sunakawa and Y. Yaguchi, Growth of β-Ga_2O_3 Single Crystals by the Edge-Defined, Film Fed Growth Method, *Jpn. J. Appl. Phys.*, 2008, **47**, 8506.
7 R. Singh, T. R. Lenka, D. K. Panda, R. T. Velpula, B. Jain, H. Q. T. Bui and H. P. T. Nguyen, The dawn of Ga_2O_3 HEMTs for high power electronics - A review, *Mater. Sci. Semicond. Process.*, 2020, **119**, 105216.
8 H. Zhou, J. Zhang, C. Zhang, Q. Feng, S. Zhao, P. Ma and Y. Hao, A review of the most recent progresses of state-of-art gallium oxide power devices, *J. Semicond.*, 2019, **40**(1), 011803.
9 M. Higashiwaki, K. Sasaki, A. Kuramata, T. Masui and S. Yamakoshi, Development of gallium oxide power devices, *Phys. Status Solidi A*, 2014, **211**(1), 21–26.
10 M. H. Wong and M. Higashiwaki, Vertical β-Ga_2O_3 power transistors: A review, *IEEE Trans. Electron Devices*, 2020, **67**(10), 3925–3937.
11 K. Konishi, K. Goto, H. Murakami, Y. Kumagai, A. Kuramata, S. Yamakoshi and M. Higashiwaki, 1-kV vertical Ga_2O_3 field-plated Schottky barrier diodes, *Appl. Phys. Lett.*, 2017, **110**(10), 103506.
12 H. Fu, H. Chen, X. Huang, I. Baranowski, J. Montes, T. H. Yang and Y. Zhao, A comparative study on the electrical properties of vertical (−201) and (010) β-Ga_2O_3 Schottky barrier diodes on EFG single-crystal substrates, *IEEE Trans. Electron Devices*, 2018, **65**(8), 3507–3513.
13 M. Higashiwaki, K. Sasaki, T. Kamimura, M. H. Wong, D. Krishnamurthy, A. Kuramata, T. Masui and S. Yamakoshi, Depletion-mode Ga_2O_3 metal-oxide-semiconductor field-effect transistors on β-Ga_2O_3 (010) substrates and temperature dependence of their device characteristics, *Appl. Phys. Lett.*, 2013, **103**, 123511.
14 M. H. Wong, K. Sasaki, A. Kuramata, S. Yamakoshi and M. Higashiwaki, Field-Plated Ga_2O_3 MOSFETs With a Breakdown Voltage of Over 750 V, *IEEE Electron Device Lett.*, 2016, **37**(2), 212–215.
15 A. J. Green, K. D. Chabak, E. R. Heller, R. C. Fitch, M. Baldini, A. Fiedler, K. Irmscher, G. Wagner, Z. Galazka, S. E. Teltak, A. Crespo, K. Leedy and G. H. Jessen, 3.8-MV/cm Breakdown Strength of MOVPE-Grown Sn-Doped β-Ga_2O_3 MOSFETs, *IEEE Electron Device Lett.*, 2016, **37**(7), 902–905.
16 S. Krishnamoorthy, Z. Xia, S. Bajaj, M. Brenner and S. Rajan, Delta-doped β-gallium oxide field-effect transistor, *Appl. Phys. Express*, 2017, **10**, 051102.
17 E. Ahmadi, O. S. Koksaldi, X. Zheng, T. Mates, Y. Oshima, U. K. Mishra and J. S. Speck, Demonstration of β-$(Al_xGa_{1-x})_2O_3$/β-Ga_2O_3 modulation doped field-effect transistors with Ge as dopant grown *via* plasma-assisted molecular beam epitaxy, *Appl. Phys. Express*, 2017, **10**, 071101.

18 N. Moser, J. McCandless, A. Crespo, K. Leedy, A. Green, A. Neal, S. Mou, E. Ahmadi, J. Speck, K. Chabak, N. Peixoto and G. Jessen, Ge-Doped β-Ga_2O_3 MOSFETs, *IEEE Electron Device Lett.*, 2017, **38**(6), 775–778.

19 M. Higashiwaki, K. Sasaki, A. Kuramata, T. Masui and S. Yamakoshi, Gallium oxide (Ga_2O_3) metal-semiconductor field-effect transistors on single-crystal β-Ga_2O_3 (010) substrates, *Appl. Phys. Lett.*, 2012, **100**, 013504.

20 K. Wang, Z. Wang, R. Cao, H. Liu, W. Chang, L. Zhao, B. Mei, H. Lv, X. Zeng and Y. Xue, Study of the mechanism of single event burnout in lateral depletion-mode Ga_2O_3 MOSFET devices *via* TCAD simulation, *J. Appl. Phys.*, 2024, **135**, 145702.

21 T. Kamimura, Y. Nakata, M. H. Wong, P. H. Than and M. Higashiwaki, Nitrogen-Doped Channel β-Ga_2O_3 MOSFET with Normally-Off Operation, in *Proceedings of 2019 Compound Semiconductor Week (CSW)*, Nara, Japan, 2019, DOI: **10.1109/ICIPRM.2019.8818991**.

22 Y. Nakata, T. Kamimura, M. H. Wong, P. H. Than, and M. Higashiwaki, Unintentional incorporation of Si and N atoms in Ga_2O_3 films grown by plasma-assisted molecular beam epitaxy, *Presented at: 61st Electronic Materials Conference (EMC 2019)*, Ann Arbor, MI, USA, 2019.

23 M. Mehta and S. Avasthi, The possibility of gallium oxide (β-Ga_2O_3) heterojunction bipolar transistors, *Phys. Scr.*, 2023, **98**, 025013.

24 E. Hossain, A. A. Rahman, M. Gokhale, R. Kulkarni, R. Mondal, A. Thamizhavel and A. Bhattacharya, Growth of high-quality GaN on (1 0 0) Ga_2O_3 substrates by facet-controlled MOVPE, *J. Cryst. Growth*, 2019, **524**, 125165.

25 S. Leone, R. Fornari, M. Bosi, V. Montedoro, L. Kirste, P. Doering, F. Benkhelifa, M. Prescher, C. Manz, V. Polyakov and O. Ambacher, Epitaxial growth of GaN/Ga_2O_3 and Ga_2O_3/GaN heterostructures for novel high electron mobility transistors, *J. Cryst. Growth*, 2020, **534**, 125511.

26 W. Y. Weng, T. J. Hsueh, S. J. Chang, G. J. Huang and H. T. Hsueh, A β-Ga_2O_3/GaN Schottky-barrier photodetector, *IEEE Photon. Technol. Lett.*, 2011, **23**, 444–446.

27 S. Nakagomi, T. Sato, Y. Takahashi and Y. Kokubun, Deep ultraviolet photodiodes based on the β- Ga_2O_3/GaN heterojunction, *Sens. Actuators, A*, 2015, **232**, 208–213.

28 R. Tang, G. Li, Y. Jiang, N. Gao, J. Li, C. Li, K. Huang, J. Kang, T. Wang and R. Zhang, Ga_2O_3/GaN heterostructural ultraviolet photodetectors with exciton-dominated ultranarrow response, *ACS Appl. Electron. Mater.*, 2021, **4**, 188–196.

29 Z. L. Xie, R. Zhang, C. T. Xia, X.-Q. Xiu, P. Han, B. Liu, H. Zhao, R.-L. Jiang, Y. Shi and Y.-D. Zheng, Demonstration of GaN/InGaN light emitting diodes on (100) β-Ga_2O_3 substrates by metalorganic chemical vapour deposition, *Chin. Phys. Lett.*, 2008, **25**, 2185.

30 C.-F. Lin, K.-T. Chen and K.-P. Huang, Blue light-emitting diodes with an embedded native gallium oxide pattern structure, *IEEE Electron Device Lett.*, 2010, **31**, 1431–1433.

31 J. Zhao, W. Li, L. Wang, X. Wei, J. Wang and T. Wei, The optical properties of InGaN/GaN nanorods fabricated on (-201) β-Ga_2O_3 substrate for vertical light emitting diodes, *Photonics*, 2021, **8**, 42.

32 H.-Y. Lee, T.-W. Chang, E. Y. Chang, N. Rorsman and C.-T. Lee, Fabrication and characterization of GaN-based fin-channel array metal-oxide-semiconductor high-electron mobility transistors with recessed-gate and Ga_2O_3 gate insulator layer, *IEEE J. Electron Devices Soc.*, 2021, **9**, 393–399.

33 M. Ge, Y. Li, Y. Zhu, D. Chen, Z. Wang and S. Tan, An improved design for e-mode AlGaN/GaN HEMT with gate stack β-Ga_2O_3/p-GaN structure, *J. Appl. Phys.*, 2021, **130**, 035703.

34 H.-Y. Lee, D.-S. Liu, J.-I. Chyi, E. Y. Chang and C.-T. Lee, Lattice-matched AlInN/GaN/AlGaN/GaN heterostructured-double-channel metal-oxide-semiconductor high-electron mobility transistors with multiple-mesa-fin-channel array, *Materials*, 2021, **14**, 5474.

35 J.-J. Jia, C.-C. Lin and C.-T. Lee, Scaling effect in gate-recessed AlGaN/GaN finnanochannel array MOSHEMTs, *IEEE Access*, 2020, **8**, 158941–158946.

36 M. Ge, Y. Li, Y. Zhu, D. Chen, Z. Wang and S. Tan, Effects of gate work function on E-mode AlGaN/GaN HEMTs with stack gate β-Ga_2O_3/p-GaN structure, *J. Phys. D Appl. Phys.*, 2021, **54**, 355103.

37 J. T. Asubar, Y. Kobayashi, K. Yoshitsugu, Z. Yatabe, H. Tokuda, M. Horita, Y. Uraoka, T. Hashizume and M. Kuzuhara, Current collapse reduction in AlGaN/GaN HEMTs by high-pressure water vapor annealing, *IEEE Trans. Electron. Dev.*, 2015, **62**, 2423–2428.

38 H. Y. Kang, M. J. Yeom, J. Y. Yang, Y. Choi, J. Lee, C. Park, G. Yoo and R. B. K. Chung, Epitaxial κ-Ga_2O_3/GaN heterostructure for high electron-mobility transistors, *Mater. Today Phys.*, 2023, **31**, 101002.

39 J.-W. Yu, Y.-R. Wu, J.-J. Huang, and L.-H. Peng, 75 GHz Ga_2O_3/GaN single nanowire metal-oxide-semiconductor field-effect transistors, in *2010 IEEE Compound Semiconductor Integrated Circuit Symposium (CSICS)*, Monterey, California, USA, 2010, pp. 1–4.

40 J.-W. Yu, Y.-R. Wu and L.-H. Peng, "Scaling of GaN single nanowire MOSFET with cutoff frequency 150 GHz, in *Gallium Nitride Materials and Devices VII*, San Francisco, California, United States, 2012, pp. 82620.

41 Y. Xu, C. Zhang, P. Yan, Z. Li, Z. Feng, Y. Zhang, D. Chen, W. Zhu, Q. Feng, S. Xu, J. Zhang and Y. Hao, Depletion-mode β-Ga_2O_3 MOSFETs grown by nonvacuum, cost-effective mist-CVD method on Fe-doped GaN substrates, *IEEE Trans. Electron. Dev.*, 2022, **69**, 1196–1199.

42 S. Hasan, M. U. Jewel, S. R. Crittenden, D. Lee, V. Avrutin, Ü. Özgür, H. Morkoç and I. Ahmad, MOCVD-grown β-Ga_2O_3 as a Gate Dielectric on AlGaN/GaN-Based Heterojunction Field Effect Transistor, *Crystals*, 2023, **13**(2), 231.

43 M. U. Jewel, S. Hasan, S. R. Crittenden, V. Avrutin, Ü. Özgür, H. Morkoç and I. Ahma, Phase stabilized MOCVD growth of β-Ga_2O_3 using SiO_x on c-plane sapphire and AlN/sapphire template, *Phys. Status Solidi A*, 2023, **220**, 2300036.

44 A. Nandi, K. S. Rana and A. Bag, Design and analysis of P-GaN/N-Ga_2O_3 based junction barrier Schottky diodes, *IEEE Trans. Electron. Dev.*, 2021, **68**, 6052–6058.

45 D. H. Mudiyanselage, D. Wang and H. Fu, Wide bandgap vertical kV-class β-Ga_2O_3/GaN heterojunction p–n power diodes with mesa edge termination, *IEEE J. Electron Devices Soc.*, 2022, **10**, 89–97.

46 J. Montes, C. Yang, H. Fu, T.-H. Yang, K. Fu, H. Chen, J. Zhou, X. Huang and Y. Zhao, Demonstration of mechanically exfoliated β-Ga_2O_3/GaN p–n heterojunction, *Appl. Phys. Lett.*, 2019, **114**, 162103.

47 Y. Liu, L. Wang, Y. Zhang, X. Dong, X. Sun, Z. Hao, Y. Luo, C. Sun, Y. Han, B. Xiong, J. Wang and H. Li, Demonstration of n-Ga_2O_3/p-GaN diodes by wet etching lift-off and transfer-print technique, *IEEE Electron Device Lett.*, 2021, **42**, 509–512.

48 P. H. Than, K. Uchida and S. Nozaki, Effects of electrical stress on the InGaP/GaAs heterojunction phototransistor, *IEEE Trans. Device Mater. Reliab.*, 2015, **15**(4), 604–609.

49 P. H. Than, K. Uchida, T. Makino, T. Ohshima and S. Nozaki, InGaP/GaAs heterojunction photosensor powered by an on-chip GaAs solar cell for energy harvesting, *Jpn. J. Appl. Phys.*, 2016, **55**, 04ES09.

50 P. H. Than, K. Uchida, T. Makino, T. Ohshima and S. Nozaki, Effects of Electrical Stress and High-Energy Electron Irradiation on the InGaP/GaAs Heterojunction Phototransistor, *MRS Online Proc. Libr.*, 2015, **1792**, 479, DOI: **10.1557/opl.2015.403**.

51 P. H. Than, T. Q. Than and Y. Takaki, Vertical p-GaN/n-Ga_2O_3 heterojunction diode with high switching performance, *Mater. Adv.*, 2025, **6**, 3139–3148.

52 P. H. Than, T. Q. Than and Y. Takaki, Breakdown voltage enhancement in p-GaAs/n-Ga_2O_3 heterojunction diodes with advanced termination designs, *Phys. Scr.*, 2025, **100**, 075022.

53 A. Y. Polyakov, N. B. Smirnov, I. V. Shchemerov, E. B. Yakimov, J. Yang, F. Ren, G. Yang, J. Kim, A. Kuramata and S. J. Pearton, Point defect induced degradation of electrical properties of Ga_2O_3 by 10 MeV proton damage, *Appl. Phys. Lett.*, 2018, **112**, 032107.

54 Z. Zhang, E. Farzana, A. R. Arehart and S. A. Ringel, Deep level defects throughout the bandgap of (010) β-Ga_2O_3 detected by optically and thermally stimulated defect spectroscopy, *Appl. Phys. Lett.*, 2016, **108**, 052105.

55 Y. Nakano, Electrical Characterization of β-Ga_2O_3 Single Crystal Substrates, *ECS J. Solid State Sci. Technol.*, 2017, **6**, 615.

56 M. E. Ingebrigtsen, J. B. Varley, A. Yu. Kuznetsov, B. G. Svensson, G. Alfieri, A. Mihaila, U. Badstübner and L. Vines, Iron and intrinsic deep level states in Ga_2O_3, *Appl. Phys. Lett.*, 2018, **112**, 042104.

57 M. Labed, N. Sengouga, C. V. Prasad, M. Henini and Y. S. Rim, On the nature of majority and minority traps in β-Ga_2O_3: A review, *Mater. Today Phys.*, 2023, **36**, 101155.

58 E. Farzana, E. Ahmadi, J. S. Speck, A. R. Arehart and S. A. Ringel, Deep level defects in Ge-doped (010) β-Ga_2O_3 layers grown by plasma-assisted molecular beam epitaxy, *J. Appl. Phys.*, 2018, **123**, 161410.

59 G. Pozina, S. Khromov, C. Hemmingsson, L. Hultman and B. Monemar, Effect of silicon and oxygen doping on donor bound excitons in bulk GaN, *Phys. Rev. B:Condens. Matter Mater. Phys.*, 2011, **84**, 165213.

60 G. A. Slack, L. J. Schowalter, M. Donald and J. A. Freitas Jr., Some effects of oxygen impurities on AlN and GaN, *J. Cryst. Growth*, 2002, **246**, 287–298.

61 A. F. Wright, Substitutional and interstitial oxygen in wurtzite GaN, *J. Appl. Phys.*, 2005, **98**, 103531.

62 C. H. Park and D. J. Chadi, Stability of deep donor and acceptor centers in GaN, AlN, and BN, *Phys. Rev. B:Condens. Matter Mater. Phys.*, 1997, **55**, 12995.

63 B. Monemar, P. P. Paskov, F. Tuomisto, K. Saarinen, M. Iwaya, S. Kamiyama, H. Amano, I. Akasaki and S. Kimura, Oxygen related shallow acceptor in GaN, *MRS Online Proc. Libr.*, 2004, **831**, 522–527.

64 B. Monemar, P. P. Paskov, F. Tuomisto, K. Saarinen, M. Iwaya, S. Kamiyama, H. Amano, I. Akasaki and S. Kimura, Dominant shallow acceptor enhanced by oxygen doping in GaN, *Phys. Rev. B:Condens. Matter Mater. Phys.*, 2006, **376–377**, 440–443.

65 Q. Feng, G. Yan, Z. Hu, Z. Feng, X. Tian, D. Jiao, W. Mu, Z. Jia, X. Lian, Z. Lai, C. Zhang, H. Zhou, J. Zhang and Y. Hao, Forward Current Conduction Mechanism of Mechanically Exfoliated β-Ga_2O_3/GaN pn Heterojunction Diode, *ECS J. Solid State Sci. Technol.*, 2020, **9**, 035001.

66 K. Xu, R. Wang, Y. Wang, J. Wang, T. Zhi, G. Yang, J. Xue, D. Chen and R. Zhang, Advances and prospects in Ga_2O_3/GaN heterojunctions: From fabrication to high-performance devices, *Mater. Sci. Semicond. Process.*, 2025, **185**, 108874.

67 Y. Zhang, Y. Li, Z. Wang, R. Guo, S. Xu, C. Liu, S. Zhao, J. Zhang and Y. Hao, Investigation of β-Ga_2O_3 films and β-Ga_2O_3/GaN heterostructures grown by metal organic chemical vapor deposition, *Sci. China Phys. Mech.*, 2020, **63**, 117311.

68 D. Seo, S. Kim, H.-Y. Kim, D.-W. Jeon, J.-H. Park and W. S. Hwang, Heteroepitaxial growth of single-crystalline β-Ga_2O_3 on GaN/Al_2O_3 using MOCVD, *Cryst. Growth Des.*, 2023, **23**, 7090–7094.

69 M. M. Muhammed, M. Peres, Y. Yamashita, Y. Morishima, S. Sato, N. Franco, K. Lorenz, A. Kuramata and I. S. Roqan, High optical and structural quality of GaN epilayers grown on (201) β-Ga_2O_3, *Appl. Phys. Lett.*, 2014, **105**, 042112.

70 J. I. Pankove, J. T. Torvik and C.-H. Qiu, Molecular doping of gallium nitride, *Appl. Phys. Lett.*, 1999, **74**, 416–418.

71 F. Ren, J. Han, R. Hickman, J. M. Van Hove, P. P. Chow, J. J. Klaassen, J. R. LaRoche, K. B. Jung, H. Cho, X. A. Cao, S. M. Donovan, R. F. Kopf, R. G. Wilson, A. G. Baca, R. J. Shul, L. Zhang, C. G. Willison, C. R. Abernathy and S. J. Pearton, GaN/AlGaN HBT fabrication, *Solid-State Electron.*, 2000, **44**, 239.

72 T. Kumabe, H. Watanabe, Y. Ando, A. Tanaka, S. Nitta, Y. Honda and H. Amano, "Regrowth-free" fabrication of high-current-gain AlGaN/GaN heterojunction bipolar

transistor with n-p-n configuration, *Appl. Phys. Express*, 2022, **15**, 046506.

73 H. Xing, P. M. Chavarkar, S. Keller, S. P. DenBaars and U. K. Mishra, Very high voltage operation (>330 V) with high current gain of AlGaN/GaN HBTs, *IEEE Electron Device Lett.*, 2003, **24**(3), 141.

74 J. B. Limb, L. McCarthy, P. Kozodoy, H. Xing, J. Ibbetson, Y. Smorchkova, S. P. DenBaars and U. K. Mishra, AlGaN/GaN HBTs using regrown emitter, *Electron. Lett.*, 1999, **35**(19), 1671.

75 L. S. McCarthy, P. Kozodoy, M. J. W. Rodwell, S. P. DenBaars and U. K. Mishra, AlGaN/GaN heterojunction bipolar transistor, *IEEE Electron Device Lett.*, 1999, **20**(6), 277.

76 Z. Lochner, H. J. Kim, Y.-C. Lee, Y. Zhang, S. Choi, S.-C. Shen, P. D. Yoder, J.-H. Ryou and R. D. Dupuis, NPN-GaN/$In_xGa_{1-x}N$/GaN heterojunction bipolar transistor on free-standing GaN substrate, *Appl. Phys. Lett.*, 2011, **99**, 193501.

77 S.-C. Shen, R. D. Dupuis, Y.-C. Lee, H.-J. Kim, Y. Zhang, Z. Lochner, P. D. Yoder and J.-H. Ryou, GaN/InGaN Heterojunction Bipolar Transistors With fT>5 GHz, *IEEE Electron Device Lett.*, 2011, **32**(8), 1065.

78 L. Zhang, X. Wang, J. Zeng, L. Jia, Z. Cheng, Y. Ai, Z. Liu, W. Tan and Y. Zhang, AlGaN/GaN Heterojunction Bipolar Transistors With High Current Gain and Low Specific ON-Resistance, *IEEE Trans. Electron Devices*, 2022, **69**(12), 6633.

79 Z. Xia, H. Xue, C. Joishi, J. McGlone, N. K. Kalarickal, S. H. Sohel, M. Brenner, A. Arehart, S. Ringel, S. Lodha, W. Lu and S. Rajan, β-Ga_2O_3 Delta-Doped Field-Effect Transistors With Current Gain Cutoff Frequency of 27 GHz, *IEEE Electron Device Lett.*, 2019, **40**(7), 1052.

80 Y. T. Tseng, C. W. Lin, W. C. Yang, K. Y. Chen and K. Y. Cheng, Influence of Al/Si Codiffusion on Current Gain Deterioration in AlGaN/GaN Single Heterojunction Bipolar Transistors, *IEEE Trans. Electron Devices*, 2016, **63**(11), 4262.

81 R. D. Dupuis, J. Kim, T.-T. Kao, Y.-C. Lee, Z. Lochner, M.-H. Ji, J.-H. Ryou, T. Detchphrom, and S.-C. Shen, Bipolar III-N high-power electronic devices, in *Proceedings Wide Bandgap Power Devices Application (WiPDA)*, Columbus, OH, USA, 2013, pp. 96–99, DOI: **10.1109/WIPDA.2013.6695571**.